Energ. Ecol. Environ. (2016) 1(1):30–38
DOI 10.1007/s40974-016-0014-y

RESEARCH ARTICLE

A useful model for solar radiation

S. A. Shehzad[1] · T. Hayat[2,3] · A. Alsaedi[3] · B. Chen[4]

[1] Department of Mathematics, Comsats Institute of Information Technology, Sahiwal 57000, Pakistan
[2] Department of Mathematics, Quaid-I-Azam University 45320, Islamabad 44000, Pakistan
[3] Nonlinear Analysis and Applied Mathematics (NAAM) Research Group, Department of Mathematics, Faculty of Science, King Abdulaziz University, Jeddah 21589, Saudi Arabia
[4] State Key Joint Laboratory of Environmental Simulation and Pollution Control, School of Environment, Beijing Normal University, Beijing 100875, People's Republic of China

Received: 21 January 2016 / Revised: 15 February 2016 / Accepted: 15 February 2016 / Published online: 26 February 2016

Abstract Energy crisis is one of the major issues of our society. There are different forms of renewable energy like wind power, geothermal energy, biomass from plants and solar energy. Solar energy is the only freely available source of renewable energy that comes directly from sun and may be converted into heat or electricity. In this article, we develop a model for solar radiation by considering the laminar flow of an incompressible Oldroyd-B fluid toward a thermally and solutally stratified moving surface with nanoparticles and thermal radiation. The data have been computed by homotopic algorithm. The computed solutions of velocity, temperature and nanoparticle concentration are plotted for multiple values of parameters of interest.

Keywords MHD · Oldroyd-B fluid · Thermal radiation · Nanoparticles · Doubly stratified stretching surface

1 Introduction

Energy has special importance in building and development of human society. The global energy is shortened in the past few decades due to rapid growth in the development of human society. The scientists and engineers across the globe are trying to find the new energy sources and new energy technologies just to meet the desired energy consumption of human beings. It is the most important source of energy which is available freely through sun. The renewable sources are geothermal energy, biomass from plants, hydropower from water and solar energy. There are serious issues in the usage of fossil fuel energy and other ordinary sources of energy to obtain the global energy requirement for the present and future. Solar energy directly comes from sun, and it can be converted into electricity and heat. Solar energy is the best candidate for renewable energy because the energy produced by it is enough for billions of years. Further, the solar energy is 2000 times higher than the consumption of human society. Hence, the implementation of solar energy has gained the special attention recently. Nanomaterial is introduced as a new energy material due to size of its particle that is smaller or equal than the de Broglie or coherent waves. Nanoparticle has an ability to absorb the incident radiation directly from sun. Such radiative characteristics of nanofluids enhance its use in thermal power systems. The implementation of nanofluids in solar system highly depends on the radiative motion of nanoparticles. There are many advantages and applications of solar energy. The renewable source of energy that never ends is solar power. Solar power has special importance in our daily life because it is a natural process of gaining water, heat and electricity with help of nature. The best source of renewable energy with minimal environmental impact is solar energy. The nanoparticles enhance the radiative properties of liquids that lead to an increase in the efficiency of direct absorption of solar collectors. Investigations through solar radiation have gained the special focus of recent researchers (Turkyilmazoglu and Pop 2013; Zheng et al. 2013; Lin et al. 2014; Shehzad et al. 2014; Mushtaq et al. 2014; Kandasamy et al. 2014; Hussain et al. 2015; Sheikholeslami et al. 2015; Hayat et al. 2015a, b).

A new class of energy transport fluids is developed by the mixture of base liquids and nanoparticles. This class of

✉ T. Hayat
fmgpak@gmail.com

liquids is called nanofluids and has popularity due to their higher thermal performance. The thermal conductivity of ordinary base fluid may be enhanced by adding the solid nanosized particles. The recent researchers are not only engaged to explore thermal properties of nanoliquids but also to develop mechanisms behind the increasing thermal efficiency that may be helpful in next-generation coolants for computers and for nuclear reactors. The mixture of nanoliquid with biotechnological components has tremendous applications in pharmaceuticals, agriculture, biological sensors, etc. The biotechnological processes involve different types of nanomaterials including nanofibers, nanowires, nanostructures, nanomachines and many others. The magnetonanoliquids are the fluids that have both magnetic and liquid characteristics. These materials have key role in optical gratings, modulators, optical switches and optical fiber filters. The magnetic nanoparticles are quite prominent in medicine, cancer therapy, tumor analysis, sink float separation, etc. The recent works on magneto nanofluids are presented in the Refs. Sheikholeslami et al. (2014a, b) Shehzad et al. (2014), Khan and Makinde (2014), Rashidi et al. (2014), Lin et al. (2015), Zhang et al. (2015), Abbasi et al. (2015), Hayat et al. (2015), Gireesha et al. (2016).

To explore the role of stratification in heat and mass transfer is current topic among the recent investigators. Stratification of fluid arises due to change in temperature and variation in concentration. It also occurs due to the presence of different types of fluids. Investigation on thermal and solutal stratification of oxygen and hydrogen in rivers is very important because these may be directly affected by the growth rate of all cultured species. The analysis of thermal stratification in solar engineering is very essential because better stratification gives high energy efficiency. The performance of system may be enhanced by the implementation of thermal stratification in energy devices. Stratified fluids are quite obvious in nature, and these occur in any heterogenous fluid body. Few examples of stratification include stratification in oceans and reservoirs, rivers, heterogenous mixture in industrial process, etc. Ibrahim and Makinde (2013) reported the impact of thermal and solutal stratification in natural convection flow of nanofluid over a flat plate. Doubly stratified flow of viscous liquid in a porous space with Soret and Dufour effects has been examined by Srinivasacharya and Surender (2014). Rashad et al. (2014) provided an analysis to explore the characteristics of thermally and solutally stratified flow of micropolar liquid in the presence of chemical reaction. Thermally radiative flow of doubly stratified Jeffrey nanofluid over a moving sheet has been addressed by Hayat et al. (2014).

The aim of this attempt is to develop a mathematical model for the renewable energy. For this purpose, we consider the solar radiation in two-dimensional flow of an Oldroyd-B fluid with nanoparticles over a stretched sheet. Solar energy at present is an important source of clean and renewable energy. The nanofluid is colloidal suspension and is uniformly dispersed in ordinary base liquid. We also incorporate the effects of double stratification. The governing nonlinear mathematical model is solved by development of homotopic algorithm (Liao 2009; Turkyilmazoglu 2010; Zheng et al. 2013; Abbasbandy et al. 2014; Abbasi et al. 2015; Hayat et al. 2015d). The results are plotted and discussed in detail for multiple values of arising parameters. The proper values of these parameters are quite essential in the industrial processes and manufacturing. The values of Deborah numbers De_1 and De_2 lie within the range of 0–1 to explore the characteristics of liquid. On the other hand side, the zero value of thermal and solutal stratification parameter corresponds to the unstratified medium. In addition, the temperature and concentration at the boundary are zero when we fix $S_T = 0 = S_C$. The values of local Nusselt and Sherwood numbers are computed numerically for multiple values of physical parameters.

2 Governing problems

An incompressible flow of an Oldroyd-B fluid over a thermally and solutally stratified stretching sheet is assumed. The considered flow is electrically conductive under the action of applied magnetic field B_0. The role of thermal radiation is encountered in the energy equations. The effects of nanoparticles are taken into account in the presence of mixed convection and heat source. The governed mathematical equations under boundary layer approach can be expressed as

$$\frac{\partial u}{\partial x}+\frac{\partial v}{\partial y}=0, \tag{1}$$

$$\begin{aligned} &u\frac{\partial u}{\partial x}+v\frac{\partial u}{\partial y}+\lambda_1\left(u^2\frac{\partial^2 u}{\partial x^2}+v^2\frac{\partial^2 u}{\partial y^2}+2uv\frac{\partial^2 u}{\partial x\partial y}\right)\\ &\quad=\nu\left(\frac{\partial^2 u}{\partial y^2}+\lambda_2\left(\begin{array}{c} u\frac{\partial^3 u}{\partial x\partial y^2}+v\frac{\partial^3 u}{\partial y^3}\\ -\frac{\partial u}{\partial x}\frac{\partial^2 u}{\partial y^2}-\frac{\partial u}{\partial y}\frac{\partial^2 u}{\partial y\partial y^2}\end{array}\right)\right)\\ &\quad-\frac{\sigma B_0^2}{\rho}u+g\beta_T((T-T_\infty)+\beta_C(C-C_\infty)), \end{aligned} \tag{2}$$

$$\begin{aligned} u\frac{\partial T}{\partial x}+v\frac{\partial T}{\partial y}&=\alpha\frac{\partial^2 T}{\partial y^2}+\tau\left(D_B\frac{\partial C}{\partial y}\frac{\partial T}{\partial y}+\frac{D_T}{T_\infty}\left(\frac{\partial T}{\partial y}\right)^2\right)\\ &\quad-\frac{1}{(\rho c)_f}\frac{\partial q_r}{\partial y}+\frac{Q}{(\rho c)_f}(T-T_\infty), \end{aligned} \tag{3}$$

$$u\frac{\partial C}{\partial x}+v\frac{\partial C}{\partial y}=D_B\frac{\partial^2 C}{\partial y^2}+\frac{D_T}{T_\infty}\frac{\partial^2 T}{\partial y^2}, \tag{4}$$

where u and v denote the velocity components in the x- and y-directions, ρ the fluid density, λ_1 the relaxation time, λ_2 the retardation time, g the gravitational acceleration, β_T the thermal expansion coefficient, β_C the concentration expansion coefficient, σ the electrical conductivity, T the fluid temperature, α the thermal diffusivity, D_B the Brownian diffusion coefficient, D_T the thermophoretic coefficient, q_r the radiative heat flux, Q the heat source/sink parameter and C the fluid concentration.

The subjected boundary conditions are

$$u = u_w(x) = cx,\ v = 0,\ T = T_w = T_0 + bx,\ C = C_w = C_0 + \mathrm{d}x \text{ at } y = 0, \tag{5}$$

$$u \to 0,\ T \to T_\infty = T_0 + ax,\ C \to C_\infty = C_0 + \mathrm{ex} \text{ as } y \to \infty. \tag{6}$$

In Eqs. (5) and (6), c denotes the stretching rate, a, b, d, e the dimensional constants and T_0 and C_0 are the reference temperature and concentration, respectively.

The radiative flux via Rosseland assumption is

$$q_r = -\frac{4\sigma^*}{3k^*}\frac{\partial T^4}{\partial y}, \tag{7}$$

where σ^* is the Stefan–Boltzmann constant and k^* the mean absorption coefficient. The differences in temperature within the flow are considered to be small such that T^4 can be described as a linear function of temperature. Expanding T^4 about T_∞ through Taylor's theorem and neglecting the higher order terms, one has

$$T^4 \cong T_\infty^4 + (T - T_\infty)4T_\infty^3 = 4T_\infty^3 T - 3T_\infty^4. \tag{8}$$

Now Eq. (4) has the following form

$$u\frac{\partial T}{\partial x} + v\frac{\partial T}{\partial y} = \alpha\frac{\partial^2 T}{\partial y^2} + \tau\left(D_B\frac{\partial C}{\partial y}\frac{\partial T}{\partial y} + \frac{D_T}{T_\infty}\left(\frac{\partial T}{\partial y}\right)^2\right) + \frac{1}{(\rho c)^f}\frac{16\sigma^* T_\infty^3}{3k^*}\frac{\partial^2 T}{\partial y^2} + \frac{Q}{(\rho c)_f}(T - T_\infty). \tag{9}$$

Setting

$$u = cxf'(\eta),\quad v = -\sqrt{c\nu}f(\eta),\quad \eta = y\sqrt{\frac{c}{\nu}},\quad \theta(\eta) = \frac{T - T_\infty}{T_w - T_0},\quad \phi(\eta) = \frac{C - C_\infty}{C_w - C_0}. \tag{10}$$

Equation (1) is satisfied identically, and other Eqs. become

$$f'''' + De_1\left(2ff'f'' - f^2f'''\right) + ff'' - f'^2 + Ha^2\beta_1 ff'' + De_2\left(f''^2 - f^2f^{iv}\right) - Ha^2f' + \lambda(\theta + N\phi) = 0, \tag{11}$$

$$\left(1 + \frac{4}{3}T_R\right)\theta'' + \Pr f\theta' + \Pr N_b\theta'\phi' + \Pr N_T\theta'^2 - \Pr f'\theta - \Pr S_T f' = 0, \tag{12}$$

$$\phi'' + \Pr Lef\phi' + (N_T/N_B)\,\theta'' - \Pr Lef'\phi - \Pr LeS_C f' = 0, \tag{13}$$

$$f = 0,\quad f' = 1,\ \theta = 1 - S_T,\ \phi = 1 - S_C \text{ at } \eta = 0, \tag{14}$$

$$f' \to 0,\ \theta \to 0,\ \phi \to 0 \text{ as } \eta \to \infty, \tag{15}$$

where $De_1 = \lambda_1 c$ is the Deborah number with respect to relaxation time, $De_2 = \lambda_2 c$ is the Deborah number with respect to retardation time, $Ha^2 = \sigma B_0^2/\rho c$ the Hartman number, $\lambda = Gr_x/\mathrm{Re}_x^2$ the thermal buoyancy parameter with $Gr_x = g\beta_T(T - T_0)x^3/\nu^2$ the local Grashof number and $Re_x = u_w(x)x/\nu$ the local Reynolds number, $\Pr = \nu/\alpha$ the Prandtl number, $Rd = \frac{4\sigma^* T_\infty^3}{kk^*}$ the thermal radiation parameter, $S_T = a/b$ the thermal stratification parameter, $S_C = e/d$ the solutal stratification parameter, $Le = \nu/D_B$ the Schmidt number and f, θ and ϕ the dimensionless velocity, temperature and nanoparticle concentration, respectively.

The dimensionless forms of local Nusselt and local Sherwood numbers can be expressed as follows:

$$Nu_x/Re_x^{1/2} = -\left(1 + \frac{4}{3}T_R\right)\theta'(0),\quad Sh_x/Re_x^{1/2} = -\phi'(0). \tag{16}$$

3 Computations

To develop the homotopic procedure (Liao 2009; Turkyilmazoglu 2010; Zheng et al. 2013; Abbasbandy et al. 2014; Abbasi et al. 2015; Hayat et al. 2015d), we choose the initial guesses and operators in the forms given below:

$$f_0(\eta) = (1 - \exp(-\eta)),\ \theta_0(\eta) = (1 - S_T)\exp(-\eta),\ \phi_0(\eta) = (1 - S_C)\exp(-\eta), \tag{17}$$

$$L(f) = f'''' - f',\quad L(\theta) = \theta'' - \theta,\quad L(\phi) = \phi'' - \phi, \tag{18}$$

with

$$L(f)(B_1 + B_2e^{\eta} + B_3e^{-\eta}) = 0,\ L(\theta)(B_4e^{\eta} + B_5e^{-\eta}) = 0,\ L(\phi)(B_5e^{\eta} + B_7e^{-\eta}) = 0, \tag{19}$$

where B_i (i = 1–7) are the arbitrary constants.

4 Analysis and discussion

Homotopy analysis method has been implemented to find the solution expressions of coupled nonlinear ordinary differential systems. It is well known that the convergence

of obtained solutions is highly reliable on the proper selection of auxiliary parameters $\hbar_f$, $\hbar_\theta$ and $\hbar_\phi$. To select the proper region of convergence, we plotted the $\hbar$-curves of functions $f(\eta)$, $\theta(\eta)$ and $\phi(\eta)$ at 21st order of approximations. The selected region of convergence lies within the ranges $-1.45 \leq \hbar_f \leq -0.05$, $-1.40 \leq \hbar_\theta \leq -0.30$ and $-1.25 \leq \hbar_\phi \leq -0.30$ (Fig. 1). Table 1 also shows that the computed homotopic solutions are convergent in the whole region of η when $\hbar_f = -0.75 = \hbar_\theta = \hbar_\phi$.

The main theme of Figs. 2, 3, 4, 5, 6, 7, 8, 9 and 10 is to visualize the role of Deborah numbers De_1 and De_2, Hartman number Ha, mixed convection parameter λ, buoyancy ratio parameter N, heat generation parameter S, radiation parameter T_R, thermal stratification parameter T_S and Brownian motion parameter N_B on the temperature distribution $\theta(\eta)$. Figure 2 shows the characteristics of Deborah number De_1 on $\theta(\eta)$. From this Fig., we evaluated that the temperature $\theta(\eta)$ and thermal boundary layer are enhanced corresponding to the increasing values of De_1. Physically, Deborah number De_1 appeared due to relaxation time, and this relaxation time is increased when De_1 enhances. Such larger relaxation time gives rise to temperature and thermal boundary layer thickness. On the other hand side, the temperature profile decays for higher values of Deborah number De_2 (see Fig. 3). This situation is arising due to appearance of retardation time in Deborah number De_2. The larger values of De_2 imply to higher retardation time that shows a reduction in temperature and thermal boundary layer thickness. The results of Maxwell fluid flow case can be retrieved by setting $De_2 = 0$. Further, the present analysis can be reduced to viscous fluid flow problem by setting $De_1 = 0 = De_2$.

The variations in temperature $\theta(\eta)$ for multiple values of Ha are shown in Fig. 4. Here, we investigated that the presence of Ha enhances the temperature $\theta(\eta)$ and its associated boundary layer thickness. The temperature profile boosts for larger Ha. This occurs due to Lorentz force which is involved in Hartman number Ha. Due to

Table 1 Convergence of homotopy solution for different order of approximations when $De_1 = 0.3$, $De_2 = 0.2$, $Ha = 0.6$, $\lambda = 0.3 = N = T_R$, $S = 0.2$, $\Pr = 1.0 = Le$, $T_S = 0.4 = C_S$ and $\hbar_f = -0.75 = \hbar_\theta = \hbar_\phi$

Order of ion approximation	$-f''(0)$	$-\theta'(0)$	$-\phi'(0)$
01	1.04200	0.57900	0.52500
08	1.03789	0.56290	0.47723
13	1.03789	0.56312	0.47747
17	1.03792	0.56315	0.47745
21	1.03792	0.56315	0.47741
28	1.03792	0.56315	0.47741
35	1.03792	0.56315	0.47741

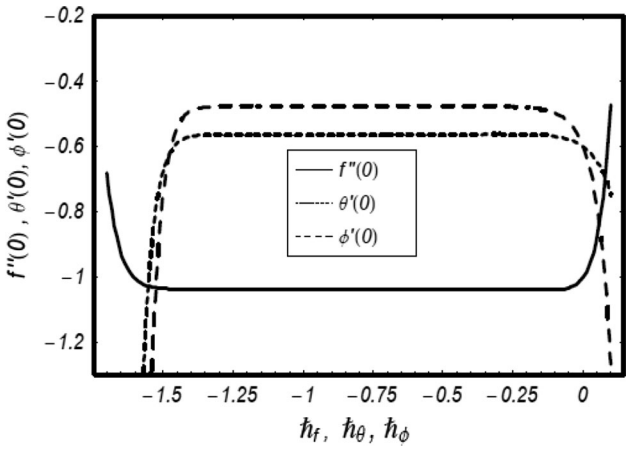

Fig. 1 Plot of $\hbar$-curves for $f(\eta)$, $\theta(\eta)$ and $\phi(\eta)$ at 22th-order of deformations when $De_1 = 0.3$, $De_2 = 0.2$, $Ha = 0.6$, $\lambda = 0.3 = N = T_R$, $S = 0.2$, $\Pr = 1.0 = Le$, $T_S = 0.4 = C_S$ and $N_B = 0.2 = N_T$

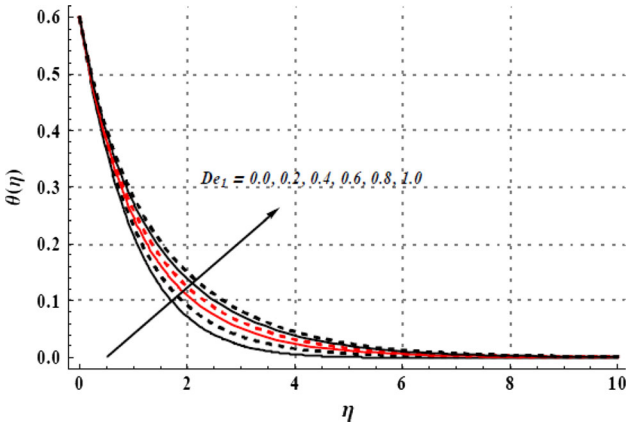

Fig. 2 Impact of De_1 on $\theta(\eta)$ when $De_2 = 0.2$, $Ha = 0.6$, $\lambda = 0.3 = N = T_R$, $S = 0.2$, $\Pr = 1.0 = Le$, $T_S = 0.4 = C_S$ and $N_B = 0.2 = N_T$

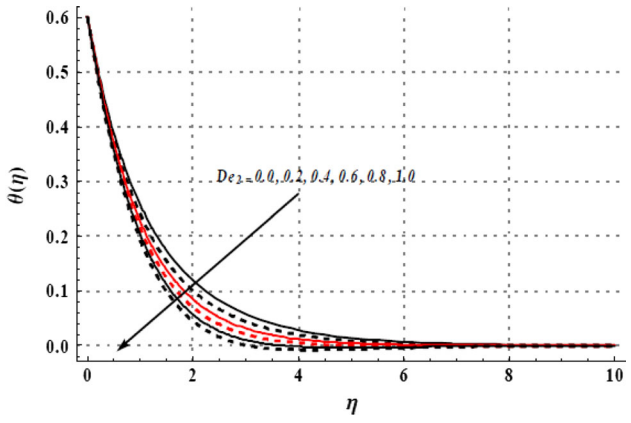

Fig. 3 Impact of De_2 on $\theta(\eta)$ when $De_1 = 0.3$, $Ha = 0.6$, $\lambda = 0.3 = N = T_R$, $S = 0.2$, $\Pr = 1.0 = Le$, $T_S = 0.4 = C_S$ and $N_B = 0.2 = N_T$

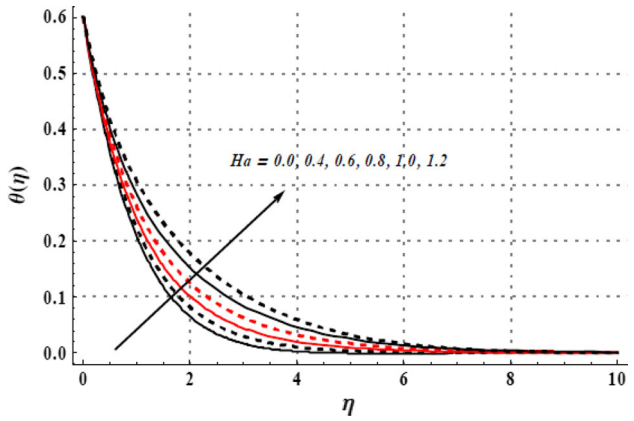

Fig. 4 Impact of Ha on $\theta(\eta)$ when $De_1 = 0.3$, $De_2 = 0.2$, $\lambda = 0.3 = N = T_R$, $S = 0.2$, $\Pr = 1.0 = Le$, $T_S = 0.4 = C_S$ and $N_B = 0.2 = N_T$

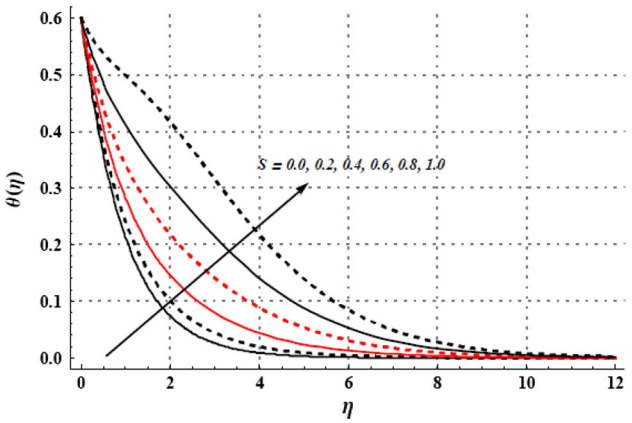

Fig. 7 Impact of S on $\theta(\eta)$ when $De_1 = 0.3$, $De_2 = 0.2$, $Ha = 0.6$, $\lambda = 0.3 = N = T_R$, $\Pr = 1.0 = Le$, $T_S = 0.4 = C_S$ and $N_B = 0.2 = N_T$

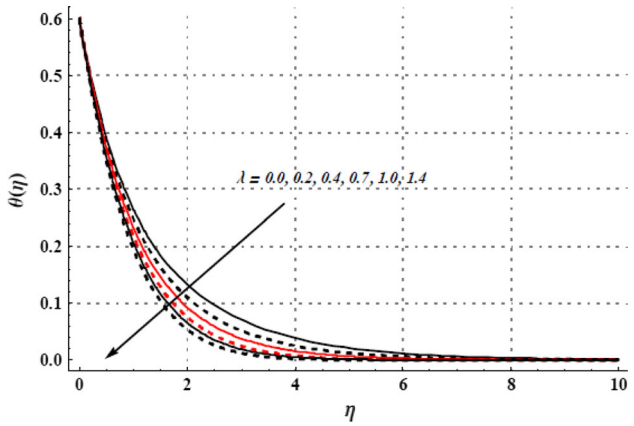

Fig. 5 Impact of λ on $\theta(\eta)$ when $De_1 = 0.3$, $De_2 = 0.2$, $Ha = 0.6$, $N = 0.3 = T_R$, $S = 0.2$, $\Pr = 1.0 = Le$, $T_S = 0.4 = C_S$ and $N_B = 0.2 = N_T$

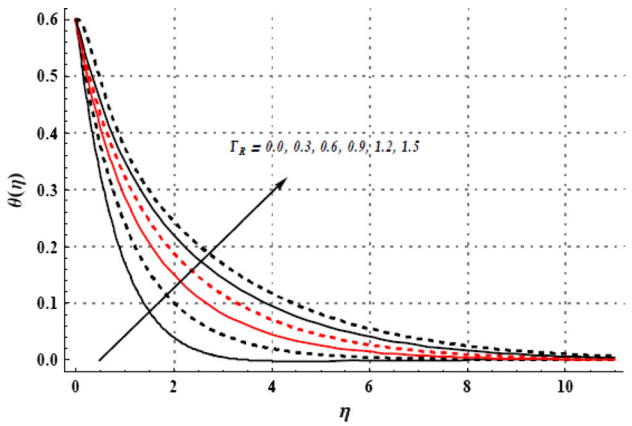

Fig. 8 Impact of T_R on $\theta(\eta)$ when $De_1 = 0.3$, $De_2 = 0.2$, $Ha = 0.6$, $\lambda = 0.3 = N$, $S = 0.2$, $\Pr = 1.0 = Le$, $T_S = 0.4 = C_S$ and $N_B = 0.2 = N_T$

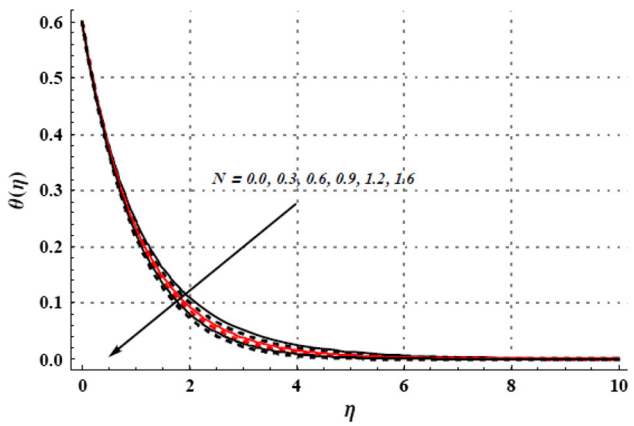

Fig. 6 Impact of N on $\theta(\eta)$ when $De_1 = 0.3$, $De_2 = 0.2$, $Ha = 0.6$, $\lambda = 0.3 = T_R$, $S = 0.2$, $\Pr = 1.0 = Le$, $T_S = 0.4 = C_S$ and $N_B = 0.2 = N_T$

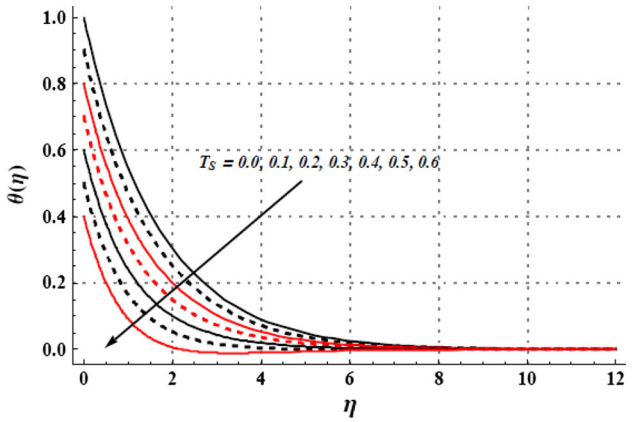

Fig. 9 Impact of T_S on $\theta(\eta)$ when $De_1 = 0.3$, $De_2 = 0.2$, $Ha = 0.6$, $\lambda = 0.3 = N = T_R$, $S = 0.2$, $\Pr = 1.0 = Le$, $C_S = 0.4$ and $N_B = 0.2 = N_T$

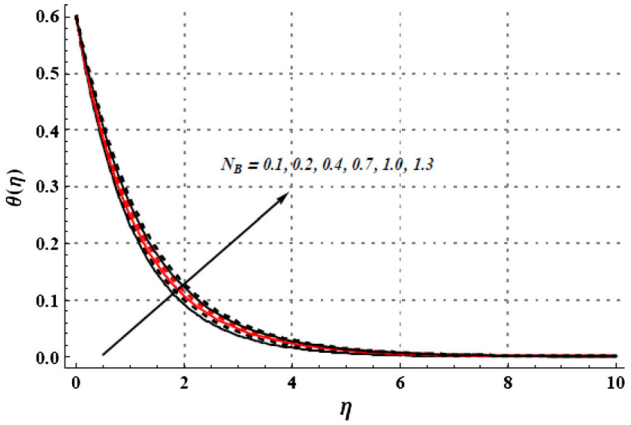

Fig. 10 Impact of N_B on $\theta(\eta)$ when $De_1 = 0.3$, $De_2 = 0.2$, $Ha = 0.6$, $\lambda = 0.3 = N = T_R$, $S = 0.2$, $\Pr = 1.0 = Le$, $T_S = 0.4 = C_S$ and $N_T = 0.2$

stronger Lorentz force, the temperature $\theta(\eta)$ is enhanced. The hydrodynamic flow case can be obtained in the absence of Ha. Figures 5 and 6 are drawn to examine the impact of mixed convection parameter λ and buoyancy ratio parameter N on the temperature $\theta(\eta)$. These Figs. clearly interpret that the temperature and its associated boundary layer thickness are smaller for larger values of λ and N. The buoyance force occurs in the definition of mixed convection and buoyancy ratio parameters. This buoyancy force is stronger corresponding to the higher mixed convection and buoyancy ratio parameters that leads to lower temperature and thinner thermal boundary layer thickness. From Fig. 7, it is revealed that an increase in heat generation parameter S enhances the temperature field significantly. More heat is produced in fluid due to an enhancement in S which gives rise to temperature and thermal boundary layer. The temperature is lower in the absence of thermal radiation (see Fig. 8). The presence of thermal radiation parameter corresponds to the thicker boundary layer thickness due to more heat absorbed by the fluid. Impact of thermal stratification S_T parameter on temperature field is shown in Fig. 9. The temperature is decreased rapidly via an increase in S_T. Higher temperature is achieved at $S_T = 0$, i.e., unstratified situation. The presence of thermal stratification reduces the effective temperature difference between the sheet and ambient fluid that shows a reduction in temperature. Figure 10 shows that the larger values of Brownian motion parameter correspond to higher temperature profile. The Brownian motion parameter appeared due to involvement of nanoparticles. Insertion of nanoparticles enhances the thermal properties of fluid due to which temperature is an increasing function of Brownian motion parameter.

The influences of Deborah numbers De_1 and De_2, Hartman number Ha, Lewis number Le, solutal stratification parameter C_S, Brownian motion parameter N_B and thermophoresis parameter N_T on nanoparticle concentration $\phi(\eta)$ are shown in Figs. 11, 12, 13, 14, 15, 16 and 17. The Deborah number De_1 enhances the nanoparticle concentration, while Deborah number De_2 reduces it (see Figs. 11, 12). It is due to reason that Deborah number De_1 is dependent on relaxation time, while Deborah number De_2 is related to retardation time. The presence of relaxation and retardation times in Deborah numbers corresponds to opposite behavior of De_1 and De_2 on nanoparticle concentration. Figure 13 shows the variations in nanoparticle concentration for multiple values of Hartman number. The nanoparticle concentration is weaker for hydrodynamic case in comparison with magnetohydrodynamic situation. The larger values of Lewis number lead to smaller nanoparticle concentration field and weaker boundary layer thickness. Physically the mass transfer at the sheet increases as we enhance the Lewis number due to which lower nanoparticle concentration profile is noticed in Fig. 14. The increase in solutal stratification parameter corresponds to a reduction in the nanoparticle concentration. Figure 15 also shows that the curve of nanoparticle concentration is higher when solutal stratification parameter is zero. From Fig. 16, we examined that the impact of Brownian motion parameter on nanoparticle concentration is highly significant for smaller values of N_B. Such variation is very weak for higher values of Brownian motion parameter. In Fig. 16, we incorporate the influence of thermophoresis parameter on nanoparticle concentration. Here, we examined that the nanoparticle concentration is enhanced gradually when we give rise to the values of thermophoresis parameter.

Table 1 shows the convergent values of $f''(0)$, $\theta'(0)$ and $\phi'(0)$ when $De_1 = 0.3$, $De_2 = 0.2 = S$, $Ha = 0.6$, $\lambda = 0.3 = N = T_R$, $\Pr = 1.0 = Le$, $T_S = 0.4 = C_S$,

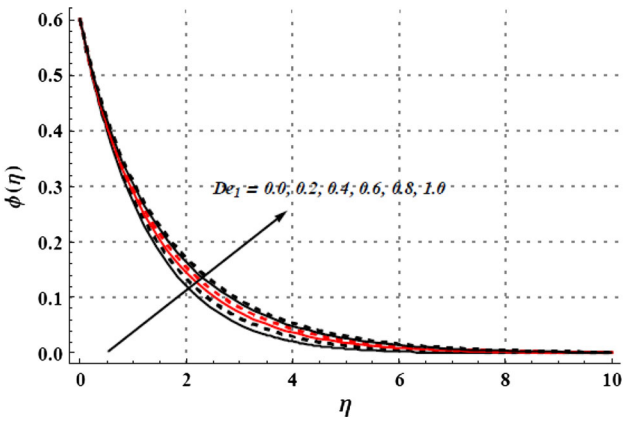

Fig. 11 Impact of De_1 on $\phi(\eta)$ when $De_2 = 0.2$, $Ha = 0.6$, $\lambda = 0.3 = N = T_R$, $S = 0.2$, $\Pr = 1.0 = Le$, $T_S = 0.4 = C_S$ and $N_B = 0.2 = N_T$

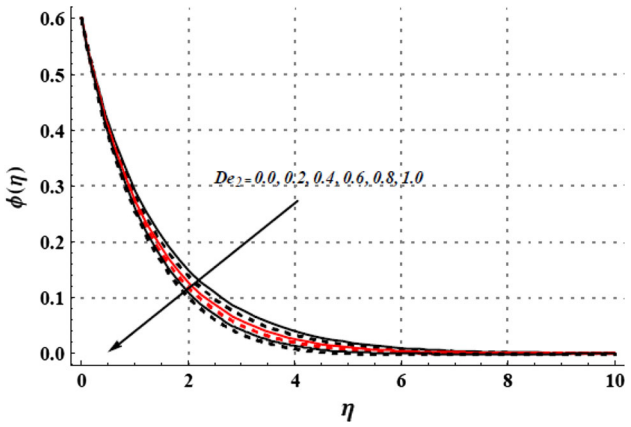

Fig. 12 Impact of De_2 on $\phi(\eta)$ when $De_1 = 0.3$, $Ha = 0.6$, $\lambda = 0.3 = N = T_R$, $S = 0.2$, $\Pr = 1.0 = Le$, $T_S = 0.4 = C_S$ and $N_B = 0.2 = N_T$

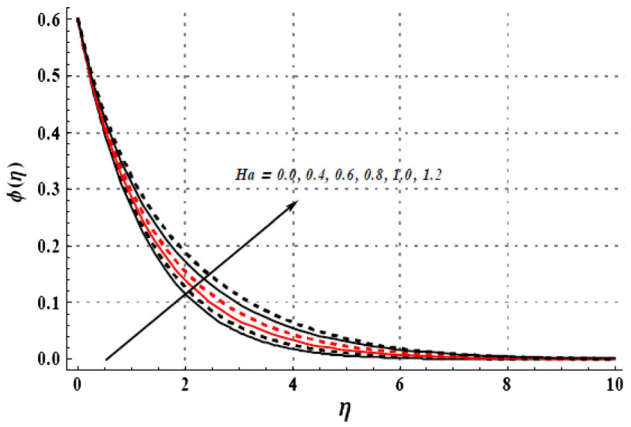

Fig. 13 Impact of Ha on $\phi(\eta)$ when $De_1 = 0.3$, $De_2 = 0.2$, $\lambda = 0.3 = N = T_R$, $S = 0.2$, $\Pr = 1.0 = Le$, $T_S = 0.4 = C_S$ and $N_B = 0.2 = N_T$

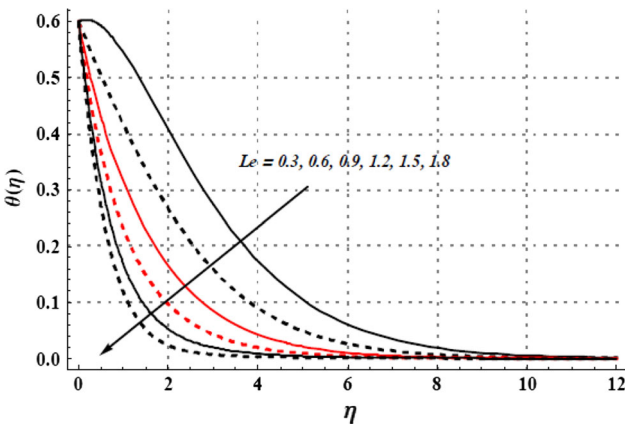

Fig. 14 Impact of Le on $\phi(\eta)$ when $De_1 = 0.3$, $De_2 = 0.2$, $Ha = 0.6$, $\lambda = 0.3 = N = T_R$, $S = 0.2$, $\Pr = 1.0$, $T_S = 0.4 = C_S$ and $N_B = 0.2 = N_T$

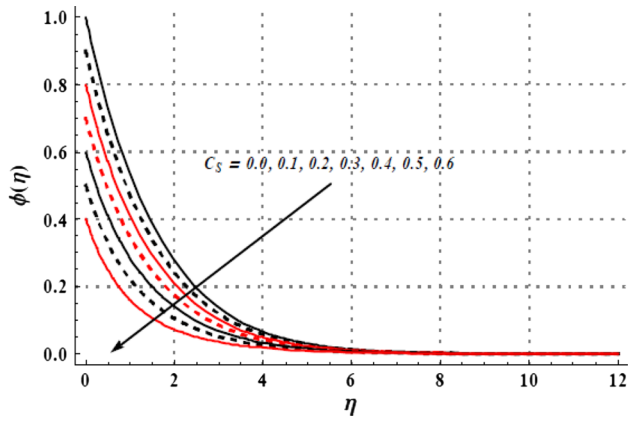

Fig. 15 Impact of C_S on $\phi(\eta)$ when $De_1 = 0.3$, $De_2 = 0.2$, $Ha = 0.6$, $\lambda = 0.3 = N = T_R$, $S = 0.2$, $\Pr = 1.0 = Le$, $T_S = 0.4$ and $N_B = 0.2 = N_T$

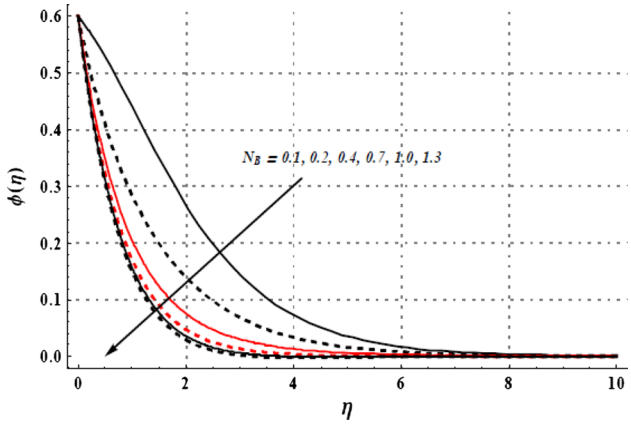

Fig. 16 Impact of N_B on $\phi(\eta)$ when $De_1 = 0.3$, $De_2 = 0.2$, $Ha = 0.6$, $\lambda = 0.3 = N = T_R$, $S = 0.2$, $\Pr = 1.0 = Le$, $T_S = 0.4 = C_S$ and $N_T = 0.2$

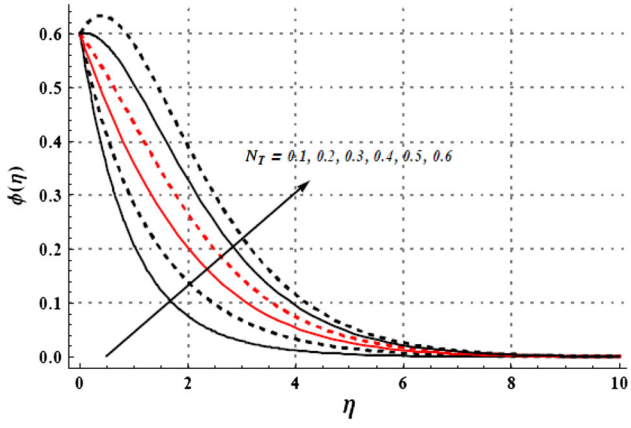

Fig. 17 Impact of N_T on $\phi(\eta)$ when $De_1 = 0.3$, $De_2 = 0.2$, $Ha = 0.6$, $\lambda = 0.3 = N = T_R$, $S = 0.2$, $\Pr = 1.0 = Le$, $T_S = 0.4 = C_S$ and $N_B = 0.2$

Table 2 Numerical computations of $\left(1+\frac{4}{3}T_R\right)\theta'(0)$ and $\phi'(0)$ for multiple values of De_1, De_2, Ha, λ, N and S when $S_C = 0.4 = S_T$, $N_B = 0.2 = N_T$, $Le = 1.0 =$ Pr and $T_R = 0.3$

De_1	De_2	Ha	λ	N	S	$-\left(1+\frac{4}{3}T_R\right)\theta'(0)$	$-\phi'(0)$
0.0	0.2	0.6	0.3	0.3	0.2	0.82816	0.49416
0.5						0.76467	0.46847
0.8						0.73260	0.45762
0.3	0.0	0.6	0.3	0.3	0.2	0.76008	0.46637
	0.3					0.80102	0.48263
	0.5					0.82384	0.49239
0.3	0.2	0.0	0.3	0.3	0.2	0.84169	0.50086
		0.4				0.81749	0.48952
		0.8				0.74936	0.46375
0.3	0.2	0.6	0.2	0.3	0.2	0.77370	0.47253
			0.6			0.81914	0.49025
			1.0			0.84792	0.50423
0.3	0.2	0.6	0.3	0.2	0.2	0.78467	0.47612
				0.6		0.79878	0.48126
				1.0		0.81103	0.48625
0.3	0.2	0.6	0.3	0.3	0.0	0.86867	0.42863
					0.1	0.83081	0.45152
					0.3	0.73772	0.50937

Table 3 Numerical computations of $\left(1+\frac{4}{3}T_R\right)\theta'(0)$ and $\phi'(0)$ for multiple values of S_C, S_T, N_B, N_T, Le, Pr and T_R when $De_1 = 0.3$, $De_2 = 0.2 = S$, $Ha = 0.6$ and $\lambda = 0.3 = N$

S_C	S_T	N_B	N_T	Le	Pr	T_R	$-\left(1+\frac{4}{3}T_R\right)\theta'(0)$	$-\phi'(0)$
0.0	0.4	0.2	0.2	1.0	1.0	0.3	0.78838	0.63382
0.5							0.78835	0.43821
0.7							0.78810	0.35983
0.4	0.0						0.87304	0.52937
	0.5						0.76295	0.46679
	0.7						0.70641	0.44926
0.4	0.4	0.1	0.2	1.0	1.0	0.3	0.81468	0.09871
		0.4					0.75121	0.66554
		0.7					0.70338	0.74622
0.4	0.4	0.2	0.1	1.0	1.0	0.3	0.79090	0.65261
			0.3				0.78558	0.30535
			0.5				0.77907	0.02857
0.4	0.4	0.2	0.2	0.8	1.0	0.3	0.79791	0.33686
				1.3			0.77885	0.66281
				2.0			0.76596	1.02204
0.4	0.4	0.2	0.2	1.0	0.8	0.3	0.68249	0.41006
					1.3		0.92891	0.57542
					2.0		1.18875	0.79797
0.4	0.4	0.2	0.2	1.0	1.0	0.0	0.70682	0.35609
						0.5	0.83157	0.53278
						0.8	0.88620	0.59454

$N_T = 0.2 = N_B$ and $\hbar_f = -0.75 = \hbar_\theta = \hbar_\phi$. This Table clearly indicates that the 21st order of HAM deformations leads to the convergent solutions. In Table 2, we computed the numerical values of local Nusselt number $\left(1+\frac{4}{3}T_R\right)\theta'(0)$ and local Sherwood number $\phi'(0)$ for multiple values of De_1, De_2, Ha, λ, N and S when $S_C = 0.4 = S_T$, $N_B = 0.2 = N_T$, $Le = 1.0 =$ Pr and $T_R = 0.3$. From this Table, we investigated that the values of local Nusselt and Sherwood numbers are smaller for larger values of Deborah number De_1, Hartman number Ha and heat source parameter S. These values are enhanced when we use the larger values of Deborah number De_2, mixed convection parameter λ and buoyancy ratio parameter N. Table 3 shows the values of $\left(1+\frac{4}{3}T_R\right)\theta'(0)$ and $\phi'(0)$ for various values of S_C, S_T, N_B, N_T, Le, Pr and T_R when $De_1 = 0.3$, $De_2 = 0.2 = S$, $Ha = 0.6$ and $\lambda = 0.3 = N$. Here, we examined that the values of $\left(1+\frac{4}{3}T_R\right)\theta'(0)$ and $\phi'(0)$ are decreased for larger values of thermal stratification parameter S_T and solutal stratification parameter S_C. However, reverse behavior of Nusselt number is observed for the increasing values of thermal radiation parameter T_R.

5 Conclusions

We explored the role of solar radiation in magnetohydrodynamic flow of an Oldroyd-B nanofluid in this work. The flow analysis is performed over thermally and solutally stratified moving surface. The heat source/sink effect is also analyzed. The governing equations of momentum, energy and mass species are coupled due to the presence of mixed convection. We found that the temperature profile is reverse for increasing values Deborah numbers De_1 and De_2. This reverse situation appeared due to the dependence of De_1 and De_2 on the relaxation and retardation times. The presence of Lorentz force in Hartman number leads to the higher temperature and nanoparticle concentration profiles. It is revealed that the effects of mixed convection parameter λ on temperature are more dominant in comparison with buoyancy ratio parameter N. The temperature and thermal boundary layer thickness are enhanced rapidly when we increase the values of thermal radiation parameter T_R. We also investigated that an increase in thermal and solutal stratification parameter leads to lower temperature and nanoparticle concentration profiles. Hence, the temperature and concentration are higher in case of unstratified surface. It is examined that the presence of nanoparticles enhances the thermal conductivity of fluid that corresponds to higher temperature.

References

Abbasbandy S, Hayat T, Alsaedi A, Rashidi MM (2014) Numerical and analytical solutions for Falkner-Skan flow of MHD Oldroyd-B fluid. Int J Numer Methods Heat Fluid Flow 24:390–401

Abbasi FM, Hayat T, Ahmad B (2015a) Peristalsis of silver-water nanofluid in the presence of Hall and Ohmic heating effects: applications in drug delivery. J Mol Liq 207:248–255

Abbasi FM, Shehzad SA, Hayat T, Alsaedi A, Obid MA (2015b) Influence of heat and mass flux conditions in hydromagnetic flow of Jeffrey nanofluid. AIP Adv 5:037111

Gireesha BJ, Mahanthesh B, Shivakumara IS, Eshwarappa KM (2016) Melting heat transfer in boundary layer stagnation-point flow of nanofluid toward a stretching sheet with induced magnetic field. Eng Sci Technol Int J 19:313–321

Hayat T, Hussain T, Shehzad SA, Alsaedi A (2014) Thermal and concentration stratifications effects in radiative flow of Jeffrey fluid. PLoS One 9:e107858

Hayat T, Imtiaz M, Alsaedi A, Kutbi MA (2015a) MHD three-dimensional flow of nanofluid with velocity slip and nonlinear thermal radiation. J Mag Mag Math 396(15):31–37

Hayat T, Muhammad T, Shehzad SA, Alsaedi A (2015b) Similarity solution to three dimensional boundary layer flow of second grade nanofluid past a stretching surface with thermal radiation and heat source/sink. AIP Adv 5:017107

Hayat T, Muhammad T, Shehzad SA, Chen GQ, Abbas IA (2015c) Interaction of magnetic field in flow of Maxwell nanofluid with convective effect. J Mag Mag Math 389:48–55

Hayat T, Muhammad T, Shehzad SA, Alhuthali MS, Lu J (2015d) Impact of magnetic field in three-dimensional flow of an Oldroyd-B nanofluid. J Mol Liq 212:272–282

Hussain T, Hayat T, Shehzad SA, Alsaedi A, Chen B (2015) A model of solar radiation and Joule heating in flow of third grade nanofluid. Z Naturforscung A 70:177–184

Ibrahim W, Makinde OD (2013) The effect of double stratification on boundary-layer flow and heat transfer of nanofluid over a vertical plate. Comput Fluids 86:433–441

Kandasamy R, Muhaimin I, Rosmila AK (2014) The performance evaluation of unsteady MHD non-Darcy nanofluid flow over a porous wedge due to renewable (solar) energy. Renew Energy 64:1–9

Khan WA, Makinde OD (2014) MHD nanofluid bioconvection due to gyrotactic microorganisms over a convectively heat stretching sheet. Int J Thermal Sci 81:118–124

Liao SJ (2009) Notes on the homotopy analysis method: some definitions and theorems. Commun Nonlinear Sci Numer Simul 14:983–997

Lin Y, Zheng L, Zhang X (2014) Radiation effects on Marangoni convection flow and heat transfer in pseudo-plastic non-Newtonian nanofluids with variable thermal conductivity. Int J Heat Mass Transf 77:708–716

Lin Y, Zheng L, Zhang X, Ma L, Chen G (2015) MHD pseudo-plastic nanofluid unsteady flow and heat transfer in a finite thin film over stretching surface with internal heat generation. Int J Heat Mass Transf 84:903–911

Mushtaq A, Mustafa M, Hayat T, Alsaedi A (2014) Nonlinear radiative heat transfer in the flow of nanofluid due to solar energy: a numerical study. J Taiwan Inst Chem Eng 45:1176–1183

Rashad AM, Abbasbandy S, Chamkha AJ (2014) Mixed convection flow of a micropolar fluid over a continuously moving vertical surface immersed in a thermally and solutally stratified medium with chemical reaction. J Taiwan Inst Chem Eng 45:2163–2169

Rashidi MM, Ganesh NV, Hakeem AKA, Ganga B (2014) Buoyancy effect on MHD flow of nanofluid over a stretching sheet in the presence of thermal radiation. J Mol Liq 198:234–238

Shehzad SA, Hayat T, Alsaedi A, Obid MA (2014a) Nonlinear thermal radiation in three-dimensional flow of Jeffrey nanofluid: a model for solar energy. Appl Math Comput 248:273–286

Shehzad SA, Abbasi FM, Hayat T, Alsaadi F (2014b) MHD mixed convective peristaltic motion of nanofluid with Joule heating and thermophoresis effects. PLoS One 9:e111417

Sheikholeslami M, Gorji-Bandpy M, Ganji DD (2014a) Lattice Boltzmann method for MHD natural convection heat transfer using nanofluid. Powder Technol 254:82–93

Sheikholeslami M, Gorji-Bandpy M, Ganji DD, Soleimani S (2014b) Heat flux boundary condition for nanofluid filled enclosure in presence of magnetic field. J Mol Liq 193:174–184

Sheikholeslami M, Ganji DD, Javed MY, Ellahi R (2015) Effect of thermal radiation on magnetohydrodynamics nanofluid flow and heat transfer by means of two phase model. J Mag Mag Math 374:36–43

Srinivasacharya D, Surender O (2014) Non-Darcy mixed convection in a doubly stratified porous medium with Soret–Dufour effects. Int J Eng Math 2014:126218

Turkyilmazoglu M (2010) A note on the homotopy analysis method. Appl Math Lett 23:1226–1230

Turkyilmazoglu M, Pop I (2013) Heat and mass transfer of unsteady natural convection flow of some nanofluids past a vertical infinite flat plate with radiation effect. Int J Heat Mass Transf 59:167–171

Zhang C, Zheng L, Zhang X, Chen G (2015) MHD flow and radiation heat transfer of nanofluids in porous media with variable surface heat flux and chemical reaction. Appl Math Model 39:165–181

Zheng L, Zhang C, Zhang X, Zhang J (2013) Flow and radiation heat transfer of a nanofluid over a stretching sheet with velocity slip and temperature jump in porous medium. J Frankl Inst 350:990–1007